https://dx.doi.org/10.1016/j.measurement.2022.110959

Measurement of covered curvature based on a tape of integrated accelerometers

Tommy Tung-Ho Hong [a], Yan Wang [a,b], Qitao Tan [a], Guoxin Zhang [a], Duo Wai-Chi Wong [a,b], and Ming Zhang [a,b,*]

[a] Department of Biomedical Engineering, Faculty of Engineering, The Hong Kong Polytechnic University, Hong Kong, China

[b] The Hong Kong Polytechnic University Shenzhen Research Institute, Shenzhen, China

*Corresponding author: Prof. Ming Zhang

Department of Biomedical Engineering, Faculty of Engineering,

The Hong Kong Polytechnic University,

Hung Hom, Kowloon,

Hong Kong, China

Email: ming.zhang@polyu.edu.hk

ABSTRACT

Quantitative measurements of spinal curvature can indicate the health of the human musculoskeletal system. However, existing measurement techniques are not feasible for unexposed back. This study used accelerometers to develop a portable, noninvasive, nonradiative, and cost-efficient device to quantitatively measure spinal curvature in real time. The measurement accuracy is approximately 99% when measuring a ø200-mm circle. Compared with the results of the three-dimensional motion analysis system, the device exhibited curvature results that were highly consistent in the Bland-Altman test (cervical lordosis angle (CLA): $r = 0.973$, thoracic kyphosis angle (TKA): $r = 0.993$, lumbar lordosis angle (LLA): $r = 0.961$, and spinal alignment trendline (SAT): $r = 0.978$). Repeatability test results: CLA = 37.63 ± 2.24°, TKA = 32.48 ± 0.98°, and LLA = 15.64 ± 1.12°. Thus, the proposed device can provide accurate and reliable quantitative measurements and can be used for spinal curvature measurements in the supine position.

Keyword: spinal curvature measurement; accelerometers by I^2C; covered curvature measurement; sensor tape; supine sleep position

Abbreviations	Nomenclature
G_{out}	Gravity output
G_{raw}	Gravity in raw data
G_x, G_y, G_z	Gravity in three axial directions
L_c	Length of chord
O_c	Zero-gravity offset deviation correction parameter
S_c	Sensitivity error correction parameter
U	Accelerometer unit
θ	Angle between two adjacent accelerometers
r	Correlation coefficient
3D	Three-dimensional
CLA	Cervical Lordosis Angle
CMT	Curvature Measurement Tape
COB	Chip-On-Board
CT	Computed Tomography
FPC	Flexible Printed Circuit
GND	Ground
GUI	Graphical User Interface
I^2C	Inter-Integrated Circuit
IMU	Inertial Measurement Unit
LGA	Land Grid Array
LLA	Lumbar Lordosis Angle
MCU	Micro Control Unit
MEMS	Micro-Electro-Mechanical Systems
MRI	Magnetic Resonance Imaging
SAT	Spinal Alignment Trendline
SCL	Serial Clock Line
SDA	Serial Data line
SMT	Surface Mount Technology
STD	Standard Deviation
TKA	Thoracic Kyphosis Angle
TPU	Thermoplastic Polyurethane
TSSOP	Thin Shrink Small Outline Package

1. Introduction

In biomechanical research, exposed surfaces can be easily measured. By contrast, measuring covered curvature is challenging. For example, spinal curvature measurement when lying on the back is difficult.

Spine posture is a crucial indicator of the health of the musculoskeletal system [1]. Correct spinal curvature ensures the least strain on related muscles, ligaments, and reasonable stress and pressure distribution in bones and joints. Spine malalignment increases the risk of muscle and ligament strain, wear of bones and joints, and pain in the neck, head, and back [2]. Measurement of spinal curvature is critical in fields such as the ergonomic design of sleeping support systems, rehabilitation, physical therapy, and orthopedics. However, accessing the spine from the back of the body is not always practical. Measurement of spinal curvature when lying on the side is easy [3]. However, limited tools have been developed for direct curvature measurement in the supine position. X-ray, computed tomography (CT), and magnetic resonance scanning (MRI) have been used in the medical assessment of spinal disorders [4,5]. However, patient radiation exposure concerns exist for these techniques. Optoelectronic, ultrasound, and other optical systems provide accurate spinal curvature measurements. However, these measurement techniques are constrained to indoor devices and require full back exposure [6–9]. Custom indentation bars are embedded in a mattress to approximate spinal curvature [10,11].

However, this method has an inherent bias because of the thickness and hardness of custom indentation bars.

Barrett's systematic review listed 15 measurements of thoracic kyphosis using cards. Measurement methods include the spinal mouse [12,13], manual inclinometer [14], digital inclinometer [15], three-dimensional (3D) ultrasound [16], photogrammetry [17,18], and spinal wheel [19]. Zhong et al. [10] used a three-layer artificial neural network model to simulate and predict the indentation curve of the human spine and established a method for predicting and evaluating the interaction between the human body and spring mattress. This measurement provides valuable information. However, an accurate quantification of the spinal curvature, especially the back in full contact with the mattress, is yet to be devised. An inertial measurement unit is feasible to noninvasively and nonradiatively measure the spinal curvature in cases of the back in an unexposed condition. Wong and Wong [20] introduced a method to monitor changes in the sitting posture using three three-axis accelerometers. Voinea et al. [21] reconstructed the posture of the human spine by using the inclination angle from five inertial sensors and a mathematical model, which can calculate and represent spinal curvature. Stollenwerk et al. [22] introduced another system consisting of five accelerometers to obtain the spinal alignment curve. These studies have detailed the potential feasibility of inertial measurement units; however, fewer sensor units were used and complex algorithms or software were required to restore curvature. Thus, the system cannot display spinal alignment in real

time, and the accuracy of this system is considerably affected by the algorithm. Large and thick units influence the accuracy of the spinal curvature when they are attached to the human back for supine sleep measurement. In this study, a thin device was proposed to measure the covered curvature accurately, flexibly, noninvasively, and nonradiatively in supine lying positions, especially under the unexposed back conditions. Therefore, multiple accelerometers were integrated to form a highly flexible thin tape based on a customized algorithm. The spinal curvature measured by this device was compared with that measured using a 3D motion-capture system to validate the design.

The contributions of the study are summarized as follows:

(1) A novel method was proposed to divide a curve into several small circular arcs that can be measured using multiple accelerometers.

(2) Connection of 30 accelerometers through a concise circuit required up to eight wires for segment internal connections and four wires for external connections.

(3) A highly customized sensor tape was developed to reduce thickness and provide flexibility.

(4) Axial tilt measurement was proposed for sensor tape twist control.

(5) Validation experiments were conducted on the proposed device.

2. Methods

In this paper, a novel curvature measurement device was developed. The design, device fabrication, including the development of hardware, software, device calibration, accuracy evaluation, and experiments for device validation is described. Moreover, the proposed device was compact, exhibited increased resolution for other applications, and rendered three-dimensional measurements possible.

2.1 Design

The schematic of the proposed curvature measurement tape (CMT) is illustrated in Fig. 1. Several sensor units (U_1–U_n) are located on the CMT; each sensor unit contains a micro-electro-mechanical system (MEMS) accelerometer that can sense the inclination. The distance between two nearby accelerometers was fixed. This flexible tape was attached to a surface and the curvature is assumed to be composed of multiple arcs, and the sensor units were located at the endpoints of the arcs. The sensor unit measures the tangent point of the arc; the arc length is defined; and the geometrical shape of the arc can be measured because the tangent angles at the start and end points of the arc and the length of the arc are known. Fig. 1 displays a curve composed of multiple arcs. The tangent angle is detected by the sensor unit as the output value of the pitch. The geometry of arc_1 is detected by accelerometer units U_1 and U_2 from their sensed inclinations $pitch_1$ and $pitch_2$. The starting point of arc_1 is (x_1, y_1), the middle point of arc_1 is (x_{1m}, y_{1m}), and the endpoint of arc_1 is at the same

point as the starting point of arc_2, which is located at (x_2, y_2). Therefore, the measured curvature was quantified using a series of coordinates.

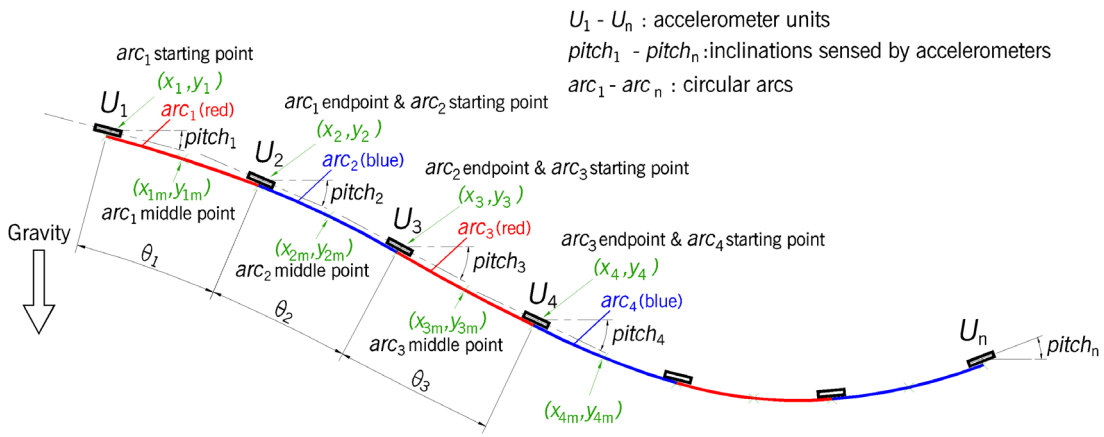

Fig. 1. Design of the curvature measurement tape (CMT).

The average length of the male spine was approximately 71 cm. The sacral and coccyx were 12.5 cm [23]. Considering the anatomical length and curvature of the human spine, the device length should be sufficiently long to cover the whole spine. Because the spine is constructed by 24 movable vertebrates and forms three natural spine angles, the use of 30 sensor units and a 30-mm sensor pitch was sufficient to detect back curvature. The width of the CMT was set to 30 mm because of ease of manufacturing, and its suitability for attachment to the human back.

2.2 Hardware development

The CMT consisted of two parts, namely a flexible sensor tape with integrated accelerometers and a control box for data processing, storage, and transmission. The two components were connected by a four-core wire for the power supply and signal transmission.

The sensor tape included 30 accelerometers, therefore, selecting an appropriate model of the accelerometer was critical. The size, resolution, accuracy, data output format, interface, and cost of parts were the criteria for model selection. Based on literature [22,24,25], ADXL345 (Analog Equipment, Wilmington, USA) was considered suitable for this project. ADXL345 is a small, thin, low-power-consumption, three-axis MEMS accelerometer with high-resolution (13-bit) measurement at up to ± 16 g. Moreover, this chip is compatible with an inter-integrated circuit (I^2C) digital interface. Although only two data wires were required for the I^2C connection, multiple devices could be connected using the I^2C interface, which renders the circuit concise. Each ADXL345 has two optional I^2C addresses (0x53 and 0x1d), which reveal that the two ADXL345 can be connected in parallel and transmit signals separately. However, this connection was insufficient for a system with 30 accelerometers. Therefore, I^2C switches (TCA9548A, Texas Instruments Inc., Texas, USA) were used. Each TCA9548A can be set to one of eight I^2C addresses from 0x70 to 0x77. The sensor tape was divided into five segments; each segment was constructed based on a customized flexible printed circuit (FPC), including an I^2C switch and six sensors. The I^2C switch communicates with the six accelerometers; all electronic parts were assembled using surface mount technology (SMT). The I^2C switch was located in the third sensor unit to minimize the number of internal connections in the segment. A wiring diagram is displayed in Fig. 2(a). The connection between the sensor units on the FPC was narrowed to ensure sensor tape

flexibility. The length of each segment was set to 180 mm, and a small tail was placed at the end of the segment, which could be connected to the beginning of another segment to form a long sensor tape. The connection of the short repetitive segments to form a complete sensor tape ensured short FPCs can be easily manufactured and maintained. The sensor tape was composed of five FPC segments with a total length of 870 mm. Based on this design, the length of the CMT can be adjusted by varying the number of segments from one to eight. Fig. 2(b) displays a close-up of an FPC segment and the sensor tape connected by the five segments.

This sensor tape should be sufficiently thin and flexible to adapt to the human back without affecting the sleeping posture. The FPC was composed of a flexible plastic substrate that provided sufficient flexibility for the sensor tape. Typically, the thickness of the FPC is 0.1 mm. The thickness of ADXL345 is 1.0 mm in land grid array packaging, and TCA9548A is 1.0 mm in thin shrink small outline package. Therefore, the maximum thickness of the electronic parts was 1.1 mm. The electronic part of the sensor tape was wrapped with a 0.2-mm-thick flexible thermoplastic polyurethane film to provide mechanical protection and waterproofing to ensure the sensor tape can be used in humid and liquid-contacting environments. Furthermore, the tape is also beneficial for sterilization. The thickness control of the sensor tape is illustrated in Fig. 2(c).

This device was developed for static data collection, which does not require a high data rate. A commonly used Arduino-compatible microcontroller (ATmega328P,

Atmel Corporation, San Jose, CA, USA) should be sufficient for data processing. The microcontroller had a built-in I^2C bus that could receive sensor data. The other modules inside the control box include a real-time clock (DS1302, Maxim Integrated, San Jose, USA), which can add a timestamp to the data. To avoid the loss of critical data, this control box contained a micro-SD adapter for local data backup. The MCU was connected to a Bluetooth module (HC-05, Maker Factory Bluetooth, Shanghai, China) for wireless data transmission (Fig. 2(d)).

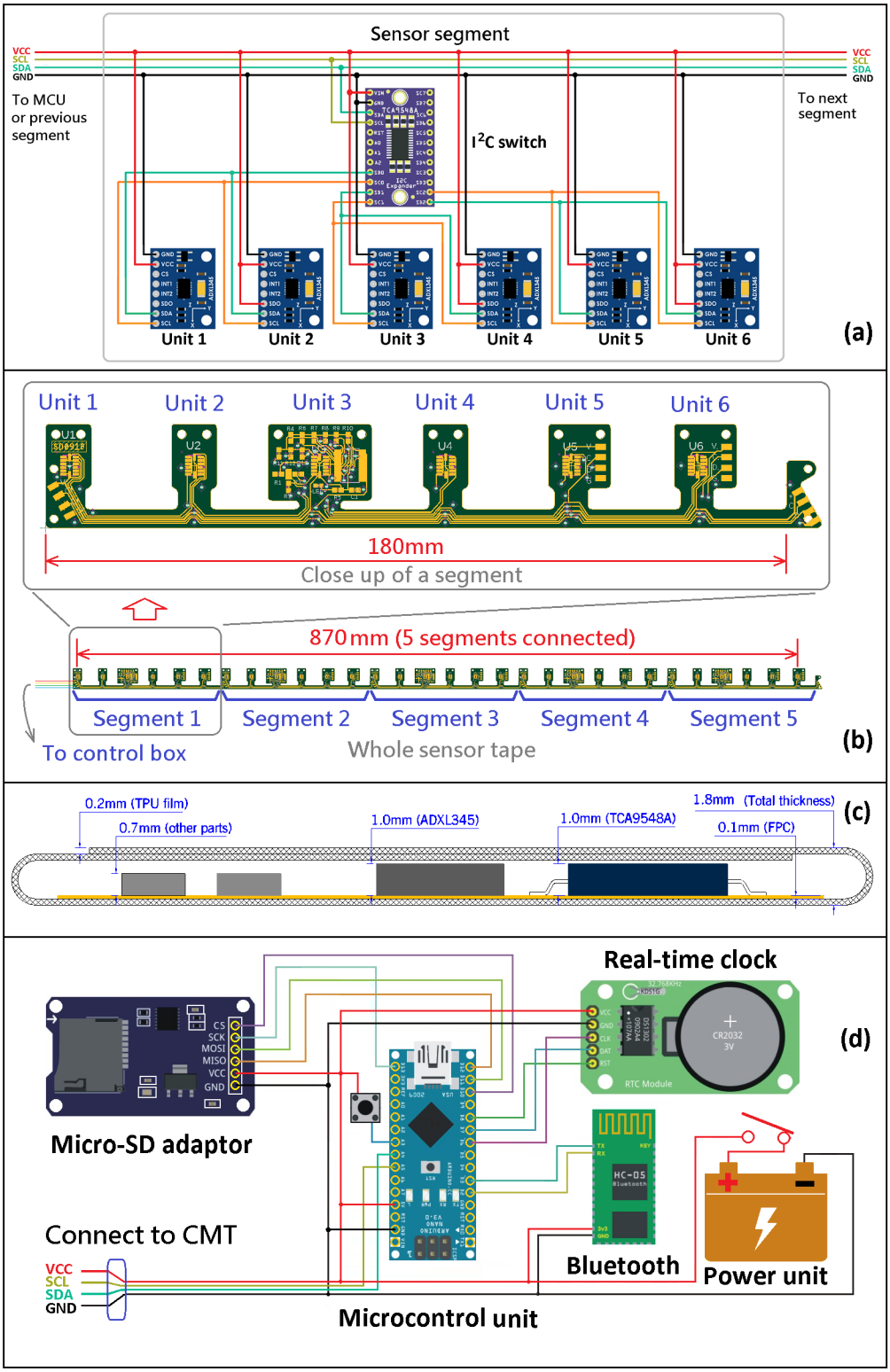

Fig. 2. Hardware development of the curvature measurement tape (CMT). (a) Wiring diagram of a segment of the sensor tape. (b) Design diagram of an FPC segment and connected sensor tape. (c) Thickness control of the sensor tape with dimension markings. (d) Wiring diagram of the control box.

SMT was used to mount electronic components on the customized FPC to fabricate the sensor tapes, and a customized PCB was used to connect the components of the control box. The housing of the control box was constructed using 3D printing. The completed CMT hardware is displayed in Fig. 3(a). The close-up of the sensor units is displayed in Fig. 3(b). The sensor tape could be easily bent under its own weight. Therefore, the sensor tape can be well attached to the surface of the measured object. However, the length of the sensor tape remained unchanged. Fig. 3(c) displays the measured thickness of the sensor tape. The area where the accelerometer is mounted has the highest thickness; however, it was just 1.8 mm in this study. The thickness of the bridge connecting the two sensor units was less than 1.0 mm.

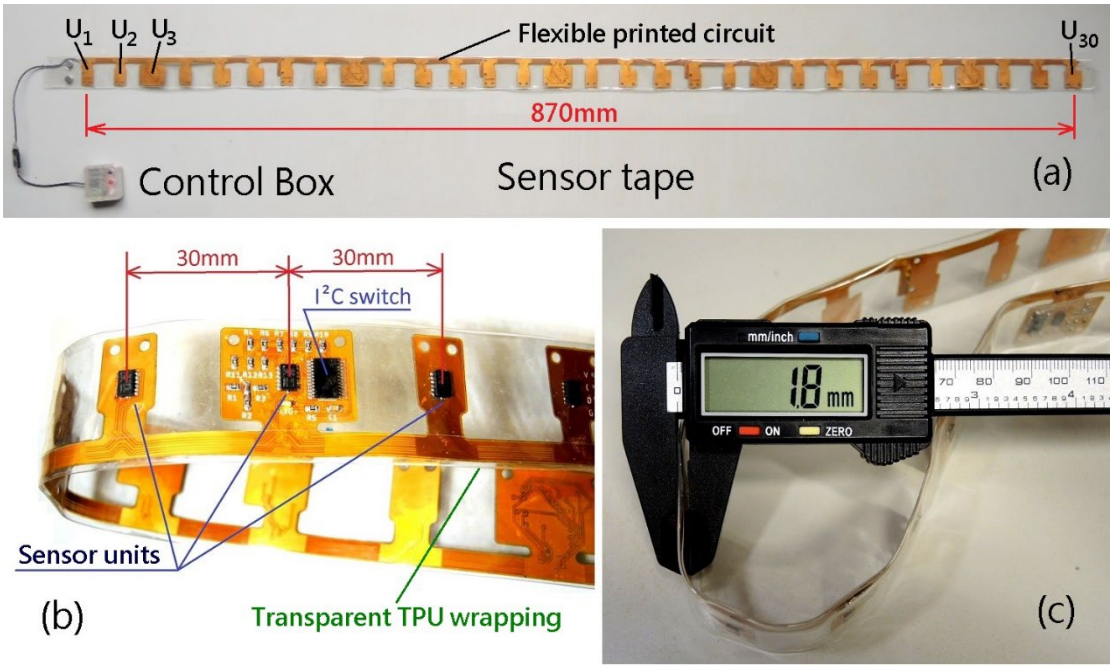

Fig. 3. Fabricated curvature measurement tape (CMT). (a) Sensor tape and control box. (b) Close-up of sensor tape. (c) Measured thickness of sensor tape.

2.3 Software development

Two software programs were used in this project. The inclination detected by the accelerometer was transmitted to the microcontroller, which performed data processing, stores it in the micro-SD card. The data were subsequently transmitted to the computer through a Bluetooth module. The received data was restored to a curve.

The Arduino program was used for microcontroller programming. The microcontroller reads the output signal of the accelerometers one at a time and corrects the deviation of each sensor. The output was converted into the Euler angle and sent through the Bluetooth module. ADXL345 has a built-in analog-to-digital converter that outputs the static acceleration of gravity in three axial directions: G_x, G_y, and G_z. The three-axis data can be converted into pitch and roll angles using Euler equations. The pitch was used to measure the tangent of the arc and it was calculated using the following equation:

$$\boldsymbol{pitch} = \mathbf{arctan}\left(\frac{G_y}{\sqrt{G_x^2+G_z^2}}\right) \quad (1)$$

The roll was used to measure the axial tilt of the sensor tape for reliability control, which was obtained using the following equation:

$$\boldsymbol{roll} = \mathbf{arctan}\left(\frac{-G_y}{G_z}\right) \quad (2)$$

The pitch and roll of this device are displayed in Fig. 4(a).

A software package with a graphical user interface was designed based on the Processing software platform (Processing 3.0, Casey Reas and Ben Fry, USA) to

process and display the curvature in real-time from the data collected through the Bluetooth interface. The distances between two adjacent accelerometers were calculated. The angle between the two accelerometers (θ) was obtained using the following equation:

$$\boldsymbol{\theta = pitch_n - pitch_{n+1}} \quad (3)$$

The distance was set to 30 mm when the sensor tape was in a straightened flat condition. This distance became the arc length in the curvature of the deformed sensor tape, as depicted in Fig. 4(b). Thus, the distance between two adjacent accelerometers, which was the chord in the curve (L_c), was calculated using the following equation:

$$\boldsymbol{L_c = \frac{sin\frac{\theta}{2} \times Arc \times 360}{\theta \times \pi}} \quad (4)$$

The two-dimensional coordinates of each accelerometer were calculated from the inclination of each accelerometer unit and the cord lengths using the following equation:

$$\boldsymbol{x_{n+1} = x_n + \cos\left(\frac{(pitch_n + pitch_{n+1}) \times \pi}{360}\right) \times L_c} \quad (5)$$

$$\boldsymbol{y_{n+1} = y_n - \sin\left(\frac{(pitch_n + pitch_{n+1}) \times \pi}{360}\right) \times L_c} \quad (6)$$

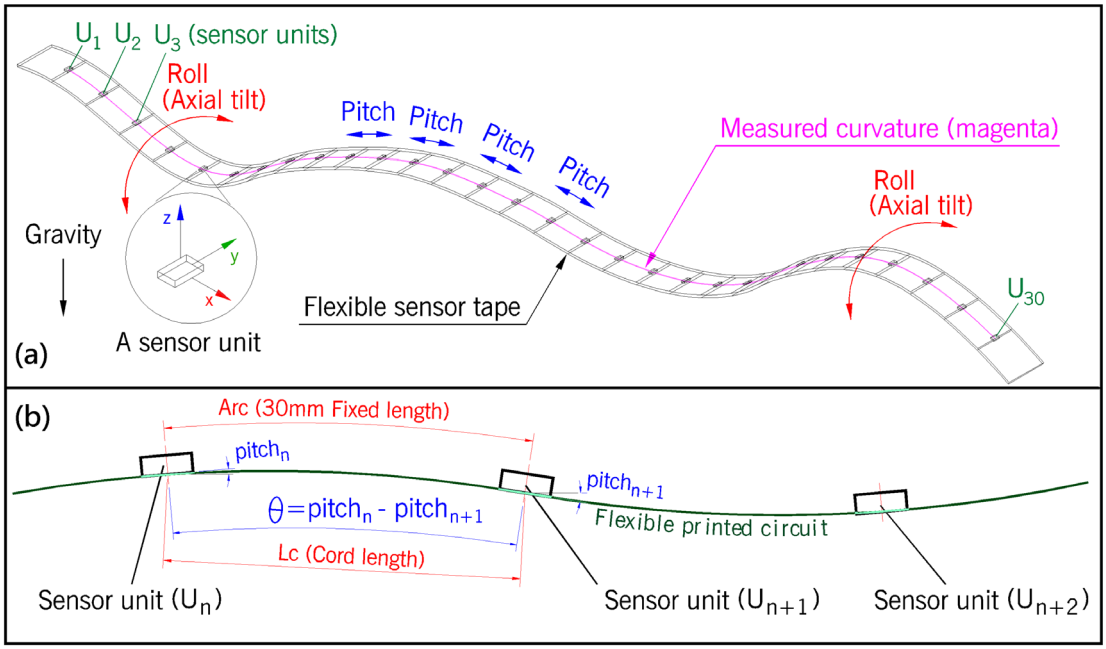

Fig. 4. Parameter labeling of the CMT. (a) The pitch and roll of the device. (b) Illustration of cord length calculation.

The coordinates are depicted as curves on a graphical user interface that represents the shape of the CMT. To facilitate subsequent data processing, software program was designed with a data input function for the experimental information, including the name of the participant, posture, body support type, and experiment time (Fig. 5(a)). The data were saved in an AutoCAD script format for further analysis. The output data presents an arc or a straight line with three points (X_{start}, Y_{start}, X_{mid}, Y_{mid}, X_{end}, and Y_{end}), and a total of 29 arcs or lines represent the entire curve. The curve displayed on the GUI was simplified, and each arc was replaced by two straight lines to reduce computational power.

Roll inclination refers to the tilt of the sensor tape along the longitudinal direction, which is the x-axis of the sensor, defined as axial tilt in this study. Because acceleratometer is unable to measure yaw, a large axial tilt could have affected the

measurement accuracy of this device, and it should be monitored. The CMT functions in a covered environment, whereas visually observing the twists of the sensors is difficult. Therefore, the system sensed the roll value of each sensor unit, displays it on the GUI, and reminded the user when an abnormal axial tilt occurred. Fig. 5(b) displays the four sensors that were manually tilted. The abnormal axial tilt of the corresponding sensors (U_7, U_8, U_9, and U_{10}) was marked at the GUI (Fig. 5(a)). A red cross was marked on the corresponding location of the curve, and the bottom of the GUI was displayed with a red square to remind the operator that an abnormal axial tilt had occurred. The range of the acceptable axial tilt was obtained by conducting a test, the test results are presented in Section 3.

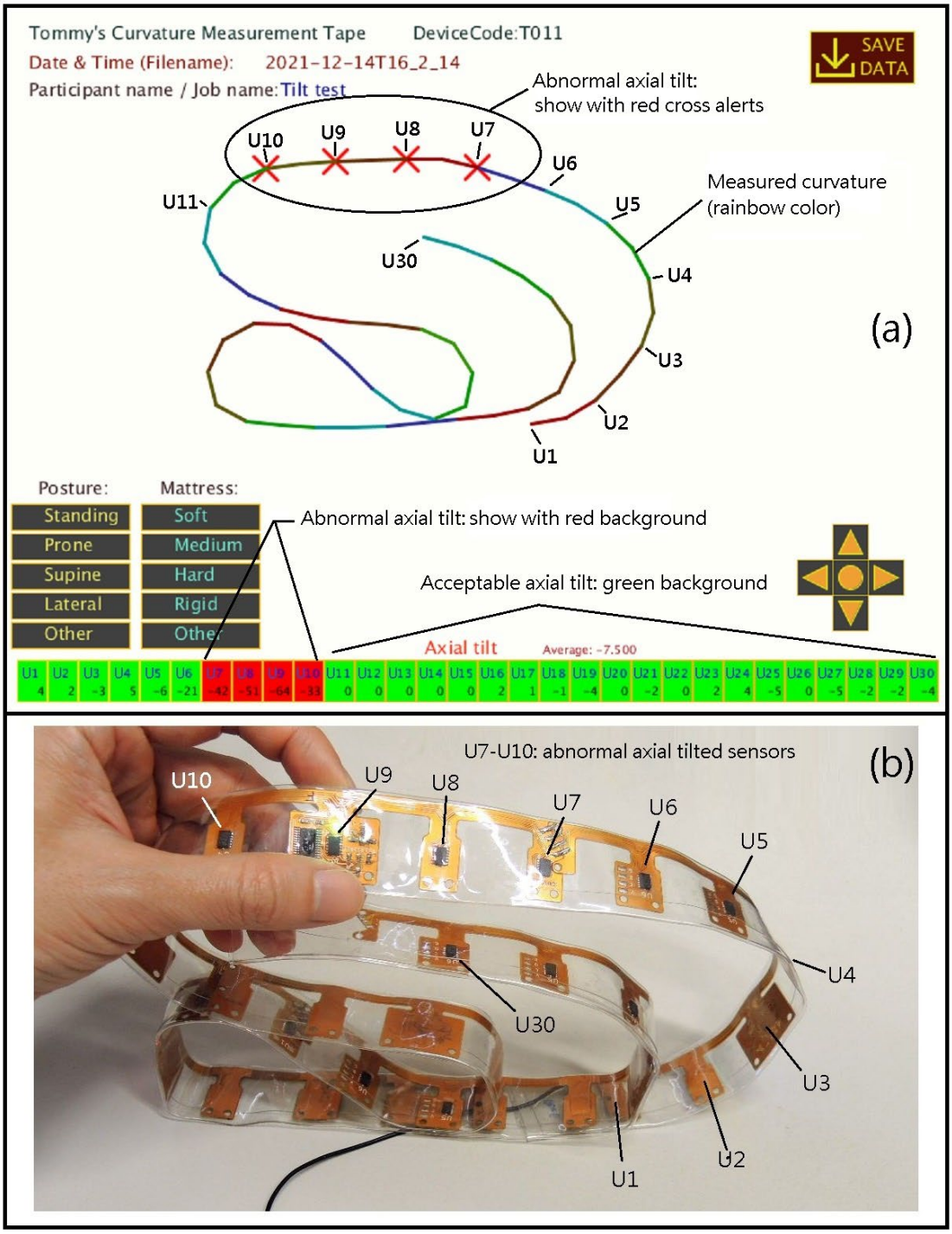

Fig. 5. Graphical user interface (GUI) and the CMT. (a) Customized GUI: The measured curvature of the sensor tape shown in (b) includes four sensors (U_7, U_8, U_9, and U_{10}) that were excessively axially tilted. (b) Sensor tape with four sensors (U_7, U_8, U_9, and U_{10}) manually excessive axial tilted.

2.4 System calibration

Because the ADXL345 accelerometer is a cost-effective low-grade MEMS inertial sensor, deviations should be compensated for before use. Sensor testing and the introduction of the datasheet revealed that the main deviations of the accelerometer included a zero-g offset and a sensitivity deviation (Fig. 6(a)). The zero-gravity offset describes the sensor readings in a zero-gravity condition; the sensitivity deviation is the instrumental error from theoretical measurements. The error of each axis was measured and compensated through the program using Equation (7). Parameter O_c was used to compensate for the zero-gravity offset deviation to ensure the sensor output became a zero value in zero gravity. The parameter S_c was used to correct the sensitivity error of the sensor so that its output value could be 256 in 1 g gravity and −256 in the case of −1 g gravity.

$$\boldsymbol{G_{out} = G_{raw} \times S_c + O_c} \quad (7)$$

Because the bottom of the sensor may not be absolutely parallel to the FPC, the SMT mounting of the accelerometer may introduce a slight angular deviation. Therefore, the assembled sensor tape was calibrated before use. The sensor tape was fixed on a rigid bar and placed horizontally, and the output data were set to zero using the program (Fig. 6(b)).

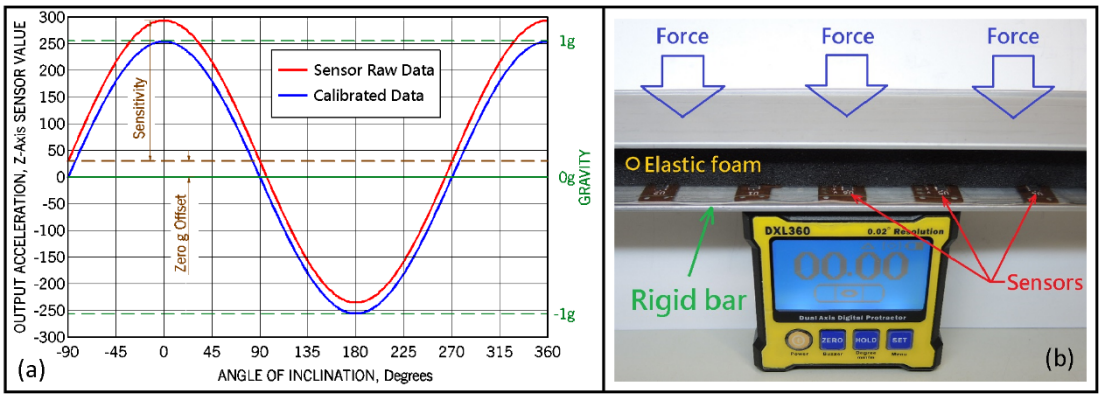

Fig. 6. Sensor calibration. (a) An example of a sensor deviation (red curve) and expected output (blue curve). (b) Design of the sensor tape calibration.

2.5 Accuracy evaluation

A 3D printed circular mount was used to test the accuracy of CMT. The sensor tape was fixed to a circular mount with a diameter of 200 mm (Fig. 7(a)). The bottom of the circular mount was installed on a digital protractor (DXL360; Jingyan, Shenzhen, China) for axial tilt monitoring (Fig. 7(b)). The circular mount could be axial tilted at a controlled angle (Fig. 7(c)). The device was tilted from 0 to 80° with 10° intervals and ± 1° accuracy to evaluate the measurement accuracy. The test results are presented in Section 3.

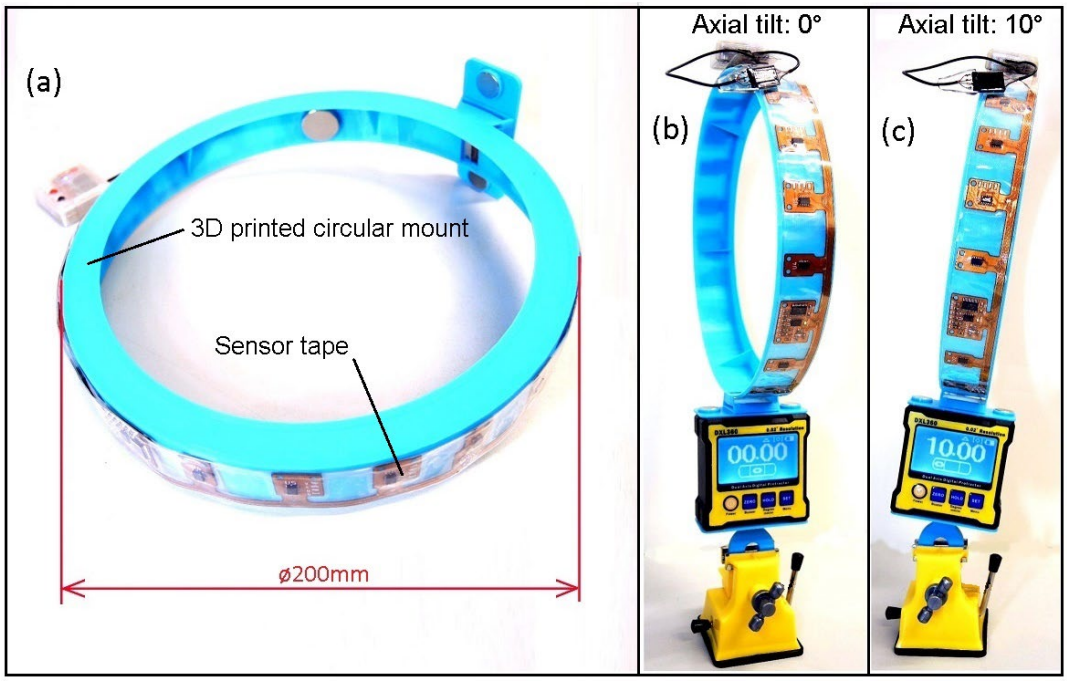

Fig. 7. Circular mount and controlled axial tilt test. (a) Prospective view of the circular mount and CMT. (b) Circular mount and CMT mounted on a digital protractor. (c) Circular mount and CMT with a 10° axial tilted placement.

2.6 Experiments

Experiments were designed to understand the reliability and repeatability of the CMT. Fifteen participants (28.6 ± 3 years) with no history of any spinal injuries, deformities, or pathologies were recruited. All participants could stand normally for more than 5 min with their arms straightened horizontally. This study was reviewed and approved by the institutional review board of the university. The reference number for ethical approvals is HSEARS 20201223001. All the participants were informed of the experimental procedures, and written informed consent for participation was obtained from them. The experiments were conducted in a human locomotion laboratory at the Hong Kong Polytechnic University. A prone sleep

experiment was performed to measure spinal curvature by using the Vicon system and CMT. The results of the two methods were compared to understand the accuracy of the proposed device for measuring spinal curvature. An eight-cameras motion-capture system (Vicon Nexus, Oxford, UK) was used for motion capture. A 5-mm-thick ethylene-vinyl acetate foam mat was placed approximately in the center of the data collection volume. The long side of the mat was parallel to the y-axis of the motion-capture system. A prone pillow (PP8320000073, ZhenZhiBao, Nanchang, China) (Fig. 8(a)) was placed on a mat to support the participants' heads.

The participants were topless, wearing tights and a customized swimming cap, and lay in a prone position on the mat, with the head supported by the prone pillow. Limbs were placed parallel to the body in the sagittal plane. The sensor tape was attached to the back along the spine, initiated from the occipital protuberance, and attached close to the whole spine until the median sacral crest (Fig. 8(b)). The CMT data were recorded and saved on a computer during the stable prone position of the participant. The sensor tape was then removed, and thirty retroreflective markers were attached to the back along the spine with the same initiated and ended points as for the sensor tape (Fig. 8(c)), with the participant remaining in the static position. The positions of the markers were recorded using a Vicon system.

From the measured curvature, a regression line called the spinal alignment tendon (SAT) was created between the occipital protuberance and the median sacral crest. The regression line represents torso angle. Other regression lines between two

adjacent bending points in the curve were created. The intersection of regression lines in the cervical spine area forms the cervical lordosis angle (CLA), the thoracic spine area forms the thoracic kyphosis angle (TKA), and that of the thoracic and lumbar spine forms the lumbar lordosis angle (LLA) (Fig. 8(d)).

The coordinates of the markers recorded in the Vicon system were the positions of the marker centers, which were approximately 7 mm away from the back, considering that the diameter of the marker was 14 mm. To maintain consistent with the CMT measurements as much as possible, the positions of the marker roots close to the back were calculated. The CLA, TKA, LLA, and SAT of the Vicon system were then calculated in similar to the calculation method used for CMT.

Another set of spinal curvatures were measured in a supine position using the CMT according to the same procedure as in the prone position. The participant lay in a supine position on a mattress (C123B, Sinomax, Shenzhen, China), with the legs straight and relaxed, and arms parallel to the legs. The head was supported using a cervical pillow (CH Pillow 1.0; Benelife, Guangzhou, China). The data collection process was performed with the participants in a supine and relaxed state. For comparison with CMT, an impression of the back geometry was obtained using a plaster bandage (P-20066, 3M Co. Ltd., St. Paul, USA) (Fig. 8(e)). The cured plaster bandage (Fig. 8(f)) was scanned using a 3D scanner (HandySCAN700, Creaform, Quebec, Canada), and the curvature of the spine was compared with CMT data.

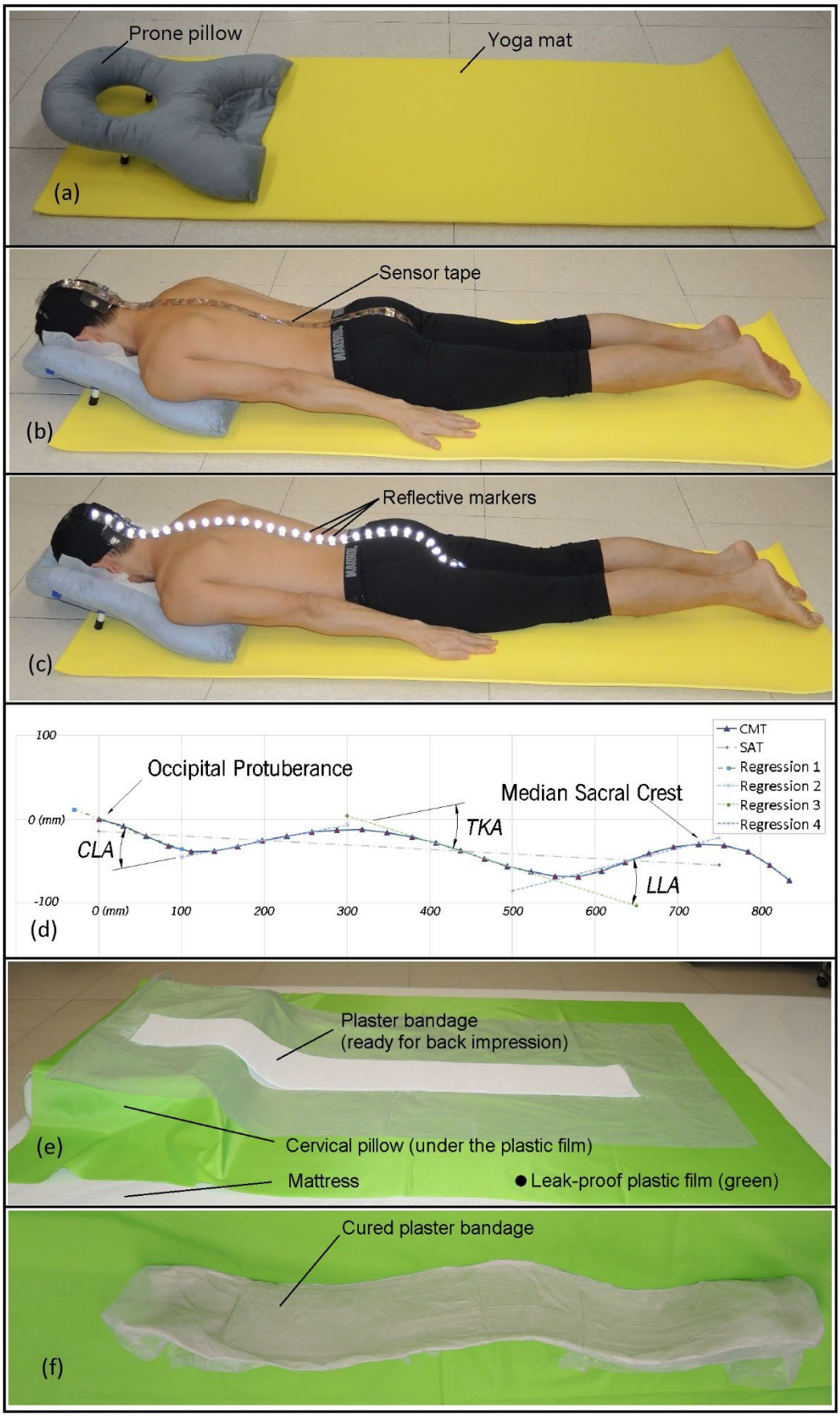
Prone pillow
Yoga mat
(a)
Sensor tape
(b)
Reflective markers
(c)
100
0 (mm)
-100
0 (mm)
100
200
300
400
500
600
700
800
Occipital Protuberance
Median Sacral Crest
CLA
TKA
LLA
CMT
SAT
Regression 1
Regression 2
Regression 3
Regression 4
(d)
Plaster bandage
(ready for back impression)
Cervical pillow (under the plastic film)
Mattress
Leak-proof plastic film (green)
(e)
Cured plaster bandage
(f)

Fig. 8. Experiment design. (a) Yoga mat and prone pillow. (b) Back curvature measurement by the CMT in a prone position. (c) Back curvature measurement by the Vicon system in a prone position. (d) Illustration of spinal curvature and related parameters. (e) Setting of the back-curvature impression in a supine position. (f) Cured plaster bandage.

3. Results

3.1 Device accuracy and precision

The CMT was fixed on a circular mount with a diameter of 200 mm (Fig. 7). The entire set was axially tilted from 0° to 80° at intervals of 10°, and ten measurements were performed at each tilt value. The CMT was randomly fixed on the mount during each measurement and removed and reinstalled after each measurement. The obtained CMT data were sent to CAD software (AutoCAD R13, Autodesk, California, USA) and restored to a curve. Ideally, the curve should represent a circle of ø 200-mm. Fig. 9 displays the curve for each tilt angle of the test. In the case of a small tilt angle, the curve almost overlapped the reference circle of ø200-mm. As the axial tilt increased, the curve was deformed. Through the measurement of the width of the curve, the mean value, and standard deviation of the curve width were used to represent the accuracy and precision of this device (Table 1).

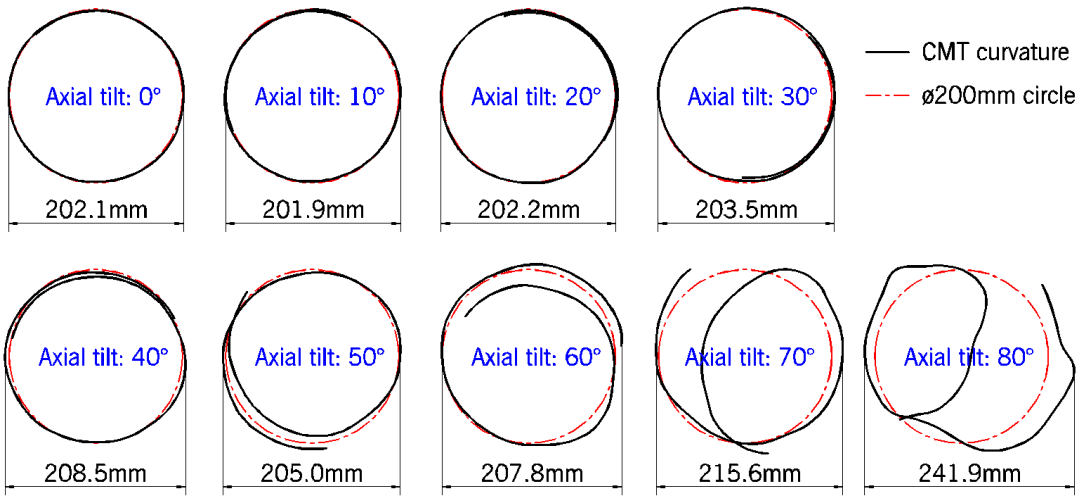

Fig. 9. Example of a measured curve of a circle at various axial tilts.

Table 1
Mean value and standard deviation of ten measurements of the width of a ø200-mm circle at various axial tilt angles.

Axial tilt	Mean (mm)	STD (mm)	Decision
0°	201.58	0.86	Acceptable
10°	201.74	0.91	
20°	201.79	1.03	
30°	201.87	1.39	
40°	202.19	2.85	Unacceptable
50°	203.05	4.09	
60°	203.67	5.06	
70°	205.87	9.69	
80°	227.77	28.45	

The CMT exhibited high accuracy and precision at an axial tilt of 0°–30°. The mean of the measured curve widths varied from 201.58 to 201.87 mm, which is approximately 99% close to the actual size of the ø200-mm circular mount. The small standard deviation value (0.85–1.39) revealed that the values in the statistical dataset were close to the mean. However, the measurement accuracy began to decline under an axial tilt of 40°. As the axial tilt increased, the measurement accuracy decreased

considerably. Therefore, the acceptance of the axial tilt angle was set to ± 30° to ensure the measurement accuracy. Any larger axial tilt is displayed in the GUI to alert the operator of an abnormality (Fig. 5(a)).

3.2 Reliability

The similarity of the CLA, TKA, LLA, and SAT parameters obtained from the device measurement and the motion-capture system were compared for CMT validation. Table 2 displays the CLA, TKA, LLA, and SAT values. The CLA was 32. 65 ± 8.21°, while the Vicon data was 32.08 ± 8.10°; The TKA was 19.90 ± 7.64°, while the Vicon data was 19.83 ± 7.13°; The LLA was 23.60 ± 6.39°, while the Vicon data 23.70 ± 7.04°. The SAT was 3.33 ± 10.68°, and the corresponding value of the Vicon data was 3.51 ± 11.10°. The results for the four parameters were all comparable between the SAS measurements and records from the motion-capture system. Correlation analysis revealed strong correlations among CLA, TKA, LLA, and SAT (CLA: $r = 0.973$, TKA: $r = 0.993$, LLA: $r = 0.961$, SAT: $r = 0.978$).

Table 2
Comparison of data obtained from the curvature measurement tape (CMT) and the motion capture system (Vicon).

	CLA		TKA		LLA		SAT	
	CMT	Vicon	CMT	Vicon	CMT	Vicon	CMT	Vicon
	(Degrees)		(Degrees)		(Degrees)		(Degrees)	
Mean	32.65	32.08	19.90	19.83	23.60	23.70	-3.21	-3.11
STD	8.21	8.10	7.64	7.13	6.39	7.04	1.98	1.94

Min.	21.88	22.89	5.69	6.43	12.70	11.15	-7.15	-6.49
Max.	51.58	51.03	30.73	30.24	34.64	35.86	0.37	0.41
r	0.973		0.993		0.961		0.978	

Fig. 10 displays the Bland-Altman plots of CLA (a), TKA (b), LLA (c), and SAT (d) of the CMT and Vicon data, respectively. The difference is normally distributed (Shapiro-Wilks P > 0.05); therefore, the Bland-Altman diagram is satisfied. Both curves revealed 95% confidence intervals (CIs).

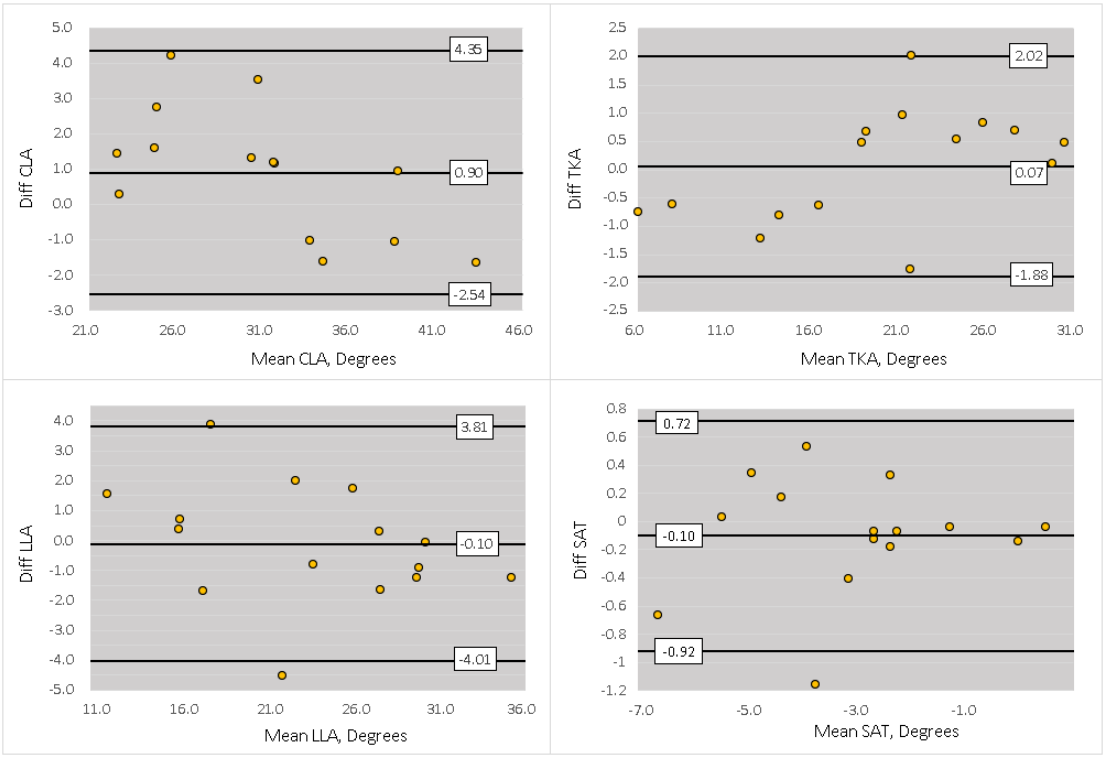

Fig. 10. Bland-Altman plot of the mean and difference of CMT and Vicon system in each participant. (a) Cervical lordosis angle (CLA). (b) Thoracic kyphosis angle (TKA). (c) Lumbar lordosis angle (LLA). (d) Spinal alignment trendline (SAT).

3.3 Repeatability

A pilot study of repeatability was performed with repeated measurements of spinal angles in the supine position. The participant's back was impressed with a plaster bandage, and the cured plaster bandage was scanned using a 3D scanner and measured using CAD software. The spine angles measured through the back impression (CLA: 36.04°, TKA: 33.15°, and LLA: 15.17°) and the angles measured by CMT (CLA: 37.63 ± 2.24°, TKA: 32.48 ± 0.98°, and LLA: 15.64 ± 1.12°) exhibited a similar trend.

4. Discussion

4.1 Importance of the study

Spinal curvature measurement in the supine position is critical [26]. However, most existing measurement methods do not provide satisfactory measurement results. Although numerous MRI scanning methods have been proposed, limitations, such as high cost and limited scan volume exists. Pins pierced mattress [11] have been used to measure spinal curvature, but it is also inefficient. Based on the proposed curvature measurement method, spinal curvature in the supine position can be easily measured. Compared with existing studies, we proposed a method to differentiate the entire curvature into multiple arcs to improve measurement accuracy. The new device had an overall thickness of 1.8 mm and was flexible. By contrast, in other studies, sensors with a thickness of 10 mm [22] were used, which considerably affects the measurement capability in the supine position; therefore, this method is not applied

[26]. First, we monitored the axial tilt of the sensor tape, and the acceptable threshold was set at ± 30°. This design avoids the occurrence of sensor twists that may occur during experiments. Experiments revealed that the accuracy of the device is acceptable for measuring spinal parameters. Overall, this study proposed a useful tool for further research on spinal curvature during sleep.

4.2 Comparison with methods in literature

The thin and flexible sensor tape exhibits limited interference with the sleep posture and is more suitable for measuring the spinal curvature in the supine position. Considerable increases in the number of sensors and newly developed algorithms result in accurate curvatures detection. However, comparing the measurement results with those reported in literature is critical. The sensor tape was installed on the ø200-mm circle mount and placed at a 0°-axial tilt (Fig. 7(b)). The measurements were repeated ten times, and the sensor tape was removed and reinstalled for each measurement. The resulting data were used in AutoCAD to draw ten curves (Fig. 11(a)). The results were compared with a ø200-mm circle, the average values from the ten curves were plotted, and the maximum error was 2.12 mm (Fig. 11(b)), an accuracy of 99%. In accordance with the literature, [21] the shape of the curve for error assessment was plotted for the wearable monitoring system. Their obtained measurements revealed that the cumulative error from the mathematical model was less than 2.5 mm or 5%. Therefore, the new device exhibited a higher measurement accuracy.

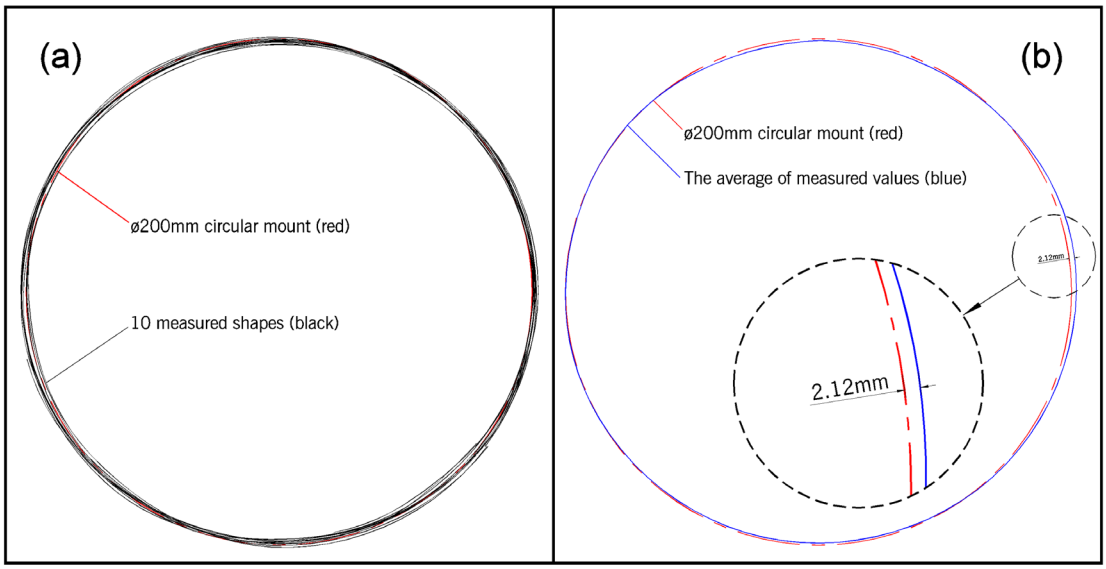

Fig. 11. (a) Visual representation of obtained results. (b) Graphical presentation of errors.

4.3 Device performance

This paper proposes a novel method for curvature measurement, which involves the use of a high degree of customized components to reduce device thickness, increase flexibility, and achieve real-time data output. The development process of the device, including hardware design and program development, is described in detail. Evaluation of the accuracy and precision of the device revealed a high accuracy in the axial tilt range of ± 30°.

The sensing length of the device was 870 mm, which can cover the entire spine of an adult male for measuring the back curvature. For females or children, the sensor belt is sufficiently long to cover the back, and the resolution remains at a certain level. Further studies should be conducted to observe the accuracy of the measurements of various age groups, sexes, and body shapes.

Accelerometers or IMUs were used to measure spinal curvature or parameters [21,27]. However, fewer sensors were used to measure the inclination angle of certain parts, which results in low accuracy [21]. Furthermore, large and bulky sensor units were used, which is not suitable for measuring the curvature of the back in the supine position. This paper proposes a novel method to connect dozens of I^2C sensors in a simple electronic circuit, a thin sensor tape based on FPC was developed, and a novel algorithm that can restore the accelerometer inclinations to a curve with high accuracy was discussed. Furthermore, the proposed method is not limited to measuring spinal curvature and can be used to measure other curvatures as well.

The sensor tape consists of 30 MEMS accelerometers, with each accelerometer priced at $3.30, including the I2C switch, microcontroller, other electronic components, and assembly costs; the device can be produced for less than $200. By contrast, an MRI scan costs more than USD 200. Furthermore, the device can be reused without any consumables. Apart from MRI scans, limited methods are used for measuring spinal curvature in the supine position. A system with pins piercing through the mattress measures the spinous process positions [11]; however, the cost for customizing the mattress by piercing the pins from the mattress top to the bottom is high. An image capture system or 3D scanner is required to capture the position of the reference markers, which are installed at the endpoint of the pins.

4.4 Length, size, and resolution

This paper proposes a design with 30 I^2C sensors connected in a simple circuit. Based on the existing circuit design, we connected eight segments, totaling 48 I^2C sensors, and confirmed that the system exhibited satisfactory performance. This study verified that a downstream pair of an I^2C switch can be connected to two devices with different I^2C addresses. Based on this circuit structure, every TCA9548A, with eight downstream pairs, can connect to 16 sensors. A device containing eight TCA9548A units can connect 128 sensors. Therefore, the length of the device reached 3810 mm, while maintaining existing resolution and measurement accuracy.

Shortening the distance of the sensor unit directly increases the measurement resolution. Based on the size of the sensor chip, the distance between the sensor units can be reduced to 10 mm. This reduction is critical in obtaining more details of the curvature.

With the use of chip-on-board technology, sensor tapes can be made narrower and thinner. The size of the accelerometer chip is approximately 2 × 2 mm [28], and if the accelerometer chip and I^2C switch are directly bonded to the FPC, the size of the sensor tape can be considerably reduced (Fig. 12(a)). This result renders it possible to measure smaller objects.

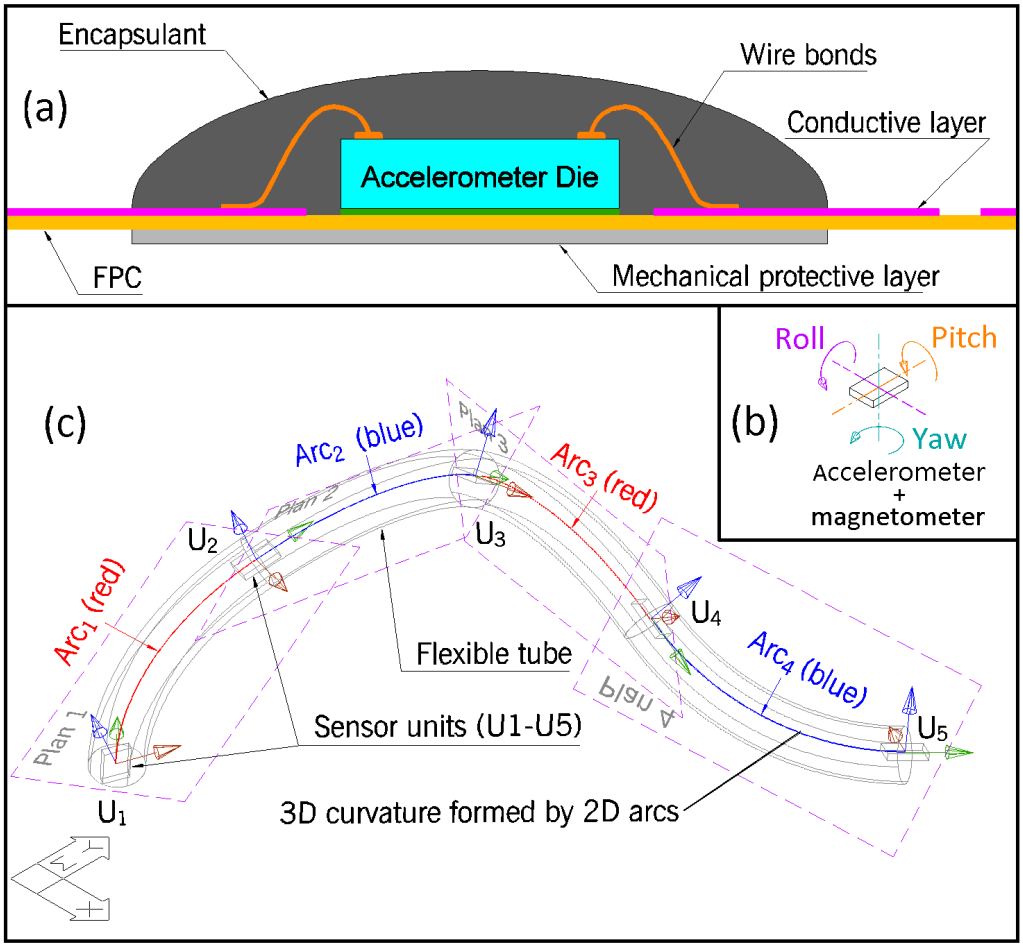

Fig. 12. (a) Mounting the accelerometer chip on the FPC to reduce the size of the sensor tape. (b) Pitch, roll, and yaw detection of a motion-traction unit. (c) Design for measurement of a three-dimensional curvature.

4.5 Three-dimensional measurement

The accelerometer can measure pitch and roll, but not yaw. The motion-traction unit (Fig. 12(b)), with an accelerometer, gyroscope, and magnetometer, can be used to detect pitch, roll, and yaw. Therefore, this design can be used for three-dimensional measurement. The sensor units were installed inside a thin tube, and the sensors were located at a fixed distance. Assuming that the tube cannot be twisted but can only be bent, two adjacent sensors are displaced in one plane. The pitch, roll, and yaw

detected by two adjacent sensor units can be used to derive the plane on which an arc can be established using sensor data (Fig. 12(c)). A nearby sensor unit creates a straight line or an arc. Multiple 2D lines or arcs can be connected to form a 3D curvature. The 3D curvature measurement method can be integrated into an endoscope as a tracking function.

5. Conclusion

A novel method is proposed for the measurement of spinal curvature in the supine position. The device accuracy, in the experiments, was approximately 99% in the measurement of a ø200-mm circle with a standard deviation of 1.39 mm. The experiments conducted on the developed device measured human spinal parameters and the results were in high agreement with a motion-capture system in the Bland-Altman test (CLA: $r = 0.973$, TKA: $r = 0.993$, LLA: $r = 0.961$, and SAT: $r = 0.978$). Repeatability tests were performed (CLA: 37.63 ± 2.24°, TKA: 32.48 ± 0.98°, and LLA: 15.64 ± 1.12°) with a plaster cast of a human back and exhibited repeatable measurements.

A device with multiple integrated accelerometers was developed and validated for noninvasive, non-radiative, and cost-efficient measurements of spinal curvature in unexposed back conditions.

Acknowledgements

We are grateful to the participants and Infinitus (China) Company Ltd. for their support of this research.

Funding

This study is supported by NFSC projects granted by the National Natural Science Foundation of China (11732015 and 11972315).

Credit Author Statement:

Tommy Tung-Ho Hong: Conceptualization, Methodology, Formal analysis, Visualization, Hardware, Software, Writing—original draft preparation, Writing—review and editing.

Yan Wang: Validation, Writing—review and editing.

Qitao Tan: Conceptualization, Validation.

Guoxin Zhang: Investigation, Data curation.

Duo Wai-Chi Wong: Methodology, Writing—review and editing.

Ming Zhang: Project administration, Resources, Funding acquisition, Writing—review and editing.

References

1. V. Verhaert, B. Haex, T. De Wilde, D. Berckmans, J. Verbraecken, E. de Valck, J.V. Sloten, Ergonomics in bed design: The effect of spinal alignment on sleep parameters, Ergonomics 54 (2) (2011) 169–178. https://doi.org/10.1080/00140139.2010.538725.
2. S. Ren, D. Wai-Chi Wong, H. Yang, Y. Zhou, J. Lin, M. Zhang, Effect of pillow height on the biomechanics of the head-neck complex: Investigation of the cranio-cervical pressure and cervical spine alignment, Peer J. 4 (2016) e2397. https://doi.org/10.7717/peerj.2397.
3. D.W.C. Wong, Y. Wang, J. Lin, Q. Tan, T.L.-W. Chen, M. Zhang, Sleeping mattress determinants and evaluation: A biomechanical review and critique, Peer J. 7 (2019) e6364. https://doi.org/10.7717/peerj.6364.
4. F. Remondino, 3-D reconstruction of static human body shape from image sequence, Comput. Vis. Image Underst. 93 (1) (2004) 65–85. https://doi.org/10.1016/j.cviu.2003.08.006.
5. R.C. Brink, D. Colo, T.P.C. Schlösser, K.L. Vincken, M. van Stralen, S.C.N. Hui, L. Shi, W.C.W. Chu, J.C.Y. Cheng, R.M. Castelein, Upright, prone, and supine spinal morphology and alignment in adolescent idiopathic scoliosis, Scoliosis Spinal Disord. 12 (2017) 6. https://doi.org/10.1186/s13013-017-0111-5.
6. S. Zhong, L. Shen, L. Zhou, Z. Guan, Predict human body indentation lying on a spring mattress using a neural network approach, Proc. Inst. Mech. Eng. H 228 (8) (2014) 787–799. https://doi.org/10.1177/0954411914547552.
7. Q. Ran, K. Zhou, Y. Yang, J. Kang, L. Zhu, Y. Tang, J. Feng, High-precision human body acquisition via multi-view binocular stereopsis, Comput. Graph. 87 (2020) 43–61. https://doi.org/10.1016/j.cag.2020.01.003.
8. G.Q. Zhou, D.-S. Li, P. Zhou, W.-W. Jiang, Y.-P. Zheng, Automating spinal curvature measurement in volumetric ultrasound via adaptive phase features, Ultrasound Med. Biol. 46 (3) (2020) 828–841. https://doi.org/10.1016/j.ultrasmedbio.2019.11.012.
9. L.R. Pivotto, I. Navarro, C.T. Candotti, Radiography and photogrammetry-based methods of assessing cervical spine posture in the sagittal plane: A systematic review with meta-analysis, Gait Posture 84 (2021) 357–367. https://doi.org/10.1016/j.gaitpost.2020.12.033.
10. J.C. Le Huec, W. Thompson, Y. Mohsinaly, C. Barrey, A. Faundez, Sagittal balance of the spine, Eur. Spine J. 28 (9) (2019) 1889–1905. https://doi.org/10.1007/s00586-019-06083-1.
11. B. Haex, J. Vander Sloten, R. Van Audekercke, Required stiffness distribution in a mattress for an optimal curvature of the human spine during bedrest, in: Computer Methods in Biomechanics & Biomedical Engineering–2, CRC Press, 2020, pp. 413–420.
12. E. Barrett, K. McCreesh, J. Lewis, Reliability and validity of non-radiographic

methods of thoracic kyphosis measurement: A systematic review, Man. Ther. 19 (1) (2014) 10–17.

13. K. Hasegawa, M. Okamoto, S. Hatsushikano, G. Caseiro, K. Watanabe, Difference in whole spinal alignment between supine and standing positions in patients with adult spinal deformity using a new comparison method with slot-scanning three-dimensional X-ray imager and computed tomography through digital reconstructed radiography, BMC Musculoskelet Disord. 19 (1) (2018) 437. https://doi.org/10.1186/s12891-018-2355-5.
14. E. Barrett, B. Lenehan, K. O'sullivan, J. Lewis, K. McCreesh, Validation of the manual inclinometer and flexicurve for the measurement of thoracic kyphosis, Physiother Theory Pract. 34 (4) (2018) 301–308. https://doi.org/10.1080/09593985.2017.1394411.
15. J. Bucke, S. Spencer, L. Fawcett, L. Sonvico, A. Rushton, N.R. Heneghan, Validity of the digital inclinometer and iPhone when measuring thoracic spine rotation, J. Athl. Train. 52 (9) (2017) 820–825. https://doi.org/10.4085/1062-6050-52.6.05.
16. T.T.-Y. Lee, J.C.-W. Cheung, S.-Y. Law, M.K.T. To, J.P.Y. Cheung, Y.-P. Zheng, Analysis of sagittal profile of spine using 3D ultrasound imaging: A phantom study and preliminary subject test, Comput. Methods Biomech. Biomed. Engin. 8 (3) (2019) 232–244. https://doi.org/10.1080/21681163.2019.1566025.
17. T.S. Furlanetto, J.A. Sedrez, C.T. Candotti, J.F. Loss, Photogrammetry as a tool for the postural evaluation of the spine: A systematic review, World J. Orthop. 7 (2) (2016) 136–148. https://doi.org/10.5312/wjo.v7.i2.136.
18. M. D'Amico, E. Kinel, P. Roncoletta, Normative 3D opto-electronic stereo-photogrammetric posture and spine morphology data in young healthy adult population, PLoS One 12 (6) (2017) e0179619. https://doi.org/10.1371/journal.pone.0179619.
19. L. Sheeran, V. Sparkes, M. Busse, R. van Deursen, Preliminary study: Reliability of the spinal wheel. A novel device to measure spinal postures applied to sitting and standing, Eur. Spine J. 19 (6) (2010) 995–1003. https://doi.org/10.1007/s00586-009-1241-0.
20. W.Y. Wong, M.S. Wong, Detecting spinal posture change in sitting positions with tri-axial accelerometers, Gait Posture, 27 (1) (2008) 168–171. https://doi.org/10.1016/j.gaitpost.2007.03.001.
21. G.D. Voinea, S. Butnariu, G. Mogan, Measurement and geometric modelling of human spine posture for medical rehabilitation purposes using a wearable monitoring system based on inertial sensors, Sensors (Basel), 17 (1) (2017) 3. https://doi.org/10.3390/s17010003
22. K. Stollenwerk, J. M¨ullers, J. M¨uller, A. Hinkenjann, B. Kr¨uger, Evaluating an accelerometer-based system for spine shape monitoring, in: Proceeding of the Computational Science and Its Applications – ICCSA 2018, Melbourne, Australia, 2018, pp. 740–756.

23. H. Gray, Anatomy of the Human Body, 29th American ed., edited by Charles Mayo Goss. With new drawings by Don M. Alvarado.. ed, ed. C.M. Goss, Lea & Febiger, Philadelphia, 1973.
24. F. Busching, U. Kulau, M. Gietzelt, L. Wolf, Comparison and validation of capacitive accelerometers for health care applications, Comput. Methods Programs Biomed. 106 (2) (2012) 79–88. https://doi.org/10.1016/j.cmpb.2011.10.009.
25. H. Yoon, S. Hwang, D. Jung, S. Choi, K. Joo, J. Choi, Y.-J.G. Lee, D. Jeong, K. Park, Estimation of sleep posture using a patch-type accelerometer based device, 37th Annual International Conference of the IEEE Engineering in Medicine and Biology Society (EMBC), 2015. https://doi.org/10.1109/EMBC.2015.7319500.
26. B. Haex, Back and Bed: Ergonomic Aspects of Sleeping, CRC Press, Boca Raton, FL (2005), pp. 103.
27. D.H. Chow, Z.Y. Ou, X.G. Wang, A. Lai, Short-term effects of backpack load placement on spine deformation and repositioning error in schoolchildren, Ergonomics, 53 (1) (2010) 56–64. https://doi.org/10.1080/00140130903389050.
28. Y. Wang, X. Zhao, D. Wen, Fabrication and characteristics of a three-axis accelerometer with double L-shaped beams, Sensors (Basel), 20 (6) (2020) 1780. https://doi.org/10.3390/s20061780.